Flood-prone areas assessment using linear binary classifiers based on flood maps obtained from 1D and 2D hydraulic models

Flood-Prone Areas Assessment Using Linear Binary Classifiers based on Flood Maps obtained from 1D and 2D Hydraulic Models

Salvatore Manfreda[1], Caterina Samela[1], Andrea Gioia[2], Giuseppe Gerardo Consoli[1], Vito Iacobellis[2], Luciana Giuzio[1], Andrea Cantisani[1] and Aurelia Sole[1]

[1] Università degli Studi della Basilicata, Via dell'Ateneo Lucano 10, Potenza, Italy.

email: salvatore.manfreda@unibas.it,

[2] Politecnico di Bari, Via E. Orabona 4, Bari, Italy.

(Last modified 10/04/2015)

ABSTRACT

The identification of flood-prone areas is a critical issue becoming everyday more pressing for our society. A preliminary delineation can be carried out by DEM-based procedures that rely on basin geomorphologic features. In the present paper, we investigated the dominant topographic controls for the flood exposure using techniques of pattern classification through linear binary classifiers based on DEM-derived morphologic features. Our findings may help the definition of new strategies for the delineation of flood-prone areas with DEM-based procedures. With this aim, local features - which are generally used to describe the hydrological characteristics of a basin - and composite morphological indices are taken into account in order to identify the most significant one. Analyses are carried out on two different datasets: one based on flood simulations obtained with a 1-D hydraulic model, and the second one obtained with a 2-D hydraulic model. The analyses highlight the potential of each morphological descriptor for the identification of the extent of flood-prone areas and, in particular, the ability of one geomorphologic index to represent flood inundated areas at different scales of application.

Keywords: flood hazard, DEM, terrain analysis, geomorphic approaches, ungauged basins.

1 INTRODUCTION

Floods, which are becoming more frequent in urban areas, are one of the natural phenomena more difficult to prevent and to deal with, especially in developing countries (Douglas et al., 2012). The remarkable number of inundations that caused, in the last decades, thousands of deaths and huge economic losses, testifies the vulnerability of many Countries to the flood hazard. On one hand, the exposure of human activities is increasing with the expansion of cities, leading to the reduction of the natural water retention capacity of the soil (e.g., Cannon, 1994; Ceola et al., 2014); on the other hand, there is a motivated suspect that the frequency of great floods is increasing with time (e.g., Milly et al., 2002; Prudhomme, 2002). The current situation is pushing the international community to find new strategies to cope with flood hazards.

The European legislation has introduced new policies for the assessment and management of flood risk for territory protection with the Floods Directive 2007/60/EC. This Directive requires Member States to assess the flood risk, mapping the flood extent over their territories, in order to evaluate assets and humans at risk, and to take adequate and coordinated measures to reduce this risk for a sustainable hydraulic protection of the territory. The European case is just an example of context where the flood risk is felt as a critical issue that should be faced, in terms of planning, at a large scale. For this reason, the definition of procedures able to provide extended description of the flood-prone areas is a growing need in Europe and several other countries. Therefore, much effort is going into the identification of flood-prone areas through the use of time-consuming hydrological/hydraulic simulations.

The patterns of flood inundations are also critical for the ecology of floodplains (Townsend et al., 1998). In fact, the temporal and spatial dynamics of floods may alter the distribution of vegetation and biodiversity of wetlands (Sharitz and Mitsch; 1993). Therefore, the accurate representation of inundation extents, as well as of surface water bodies, is crucial for the management and conservation of wetland ecosystems (Nei et al., 2009; Bridgham et al., 2013).

In this framework, the research has recently shown that the delineation of flood-prone areas can be carried out using simplified methods that rely on basin geomorphologic features (e.g., Nardi et al., 2006; Manfreda et al., 2011; Degiorgis et al., 2012; Manfreda et al., 2014a; Jalayer et al., 2014; De Risi et al., 2014; Papaioannou et al., 2014). Such innovative procedures may provide a preliminary delineation of the flood-prone areas useful for the planning of numerical analyses, and for insurance companies that have a growing interest toward the identification of the assets and population at risk.

This kind of approach may be extremely beneficial in the definition of new procedures for the identification of flooded areas from remote sensing techniques, where the topographic information may be used as external constraint in the adopted algorithms, that generally rely only on the local slope or the distance to the channel (e.g., Brivio et al., 2002). For instance, Fluet-Chouinard et al. (2014) used the topographic information to generate inundation probability maps for downscaling course-scale remote sensing data.

In particular, Degiorgis et al. (2012) introduced the use of linear binary classifiers to investigate the relationships between several morphological features and the flooding hazard at the catchment scale. In the present work, we extend the number of morphological features investigated, using single local features as well as composite indices (built with the specific aim to represent a metric of flood hazard) derived from Digital Elevation Models (DEMs).

The performances of the selected morphological features on the Bradano River (Southern Italy) are evaluated at different scales of application, using two reference flood inundation maps: one obtained applying a mono-dimensional approach over the entire basin (basin scale) and one obtained using a two-dimensional approach at the basin outlet (local scale). This last represents an extremely interesting study case that has never been considered for geomorphic applications. In fact, most of the applications made since now have only compared morphological features with mono-dimensional simulations over mountainous areas, but it is well known that the most challenging problem for hydraulic studies is represented by flat areas. Hence, the main motivation for this study is the identification of a metric suitable for both mountainous and flat areas.

In recent studies, the best-performing local features, among those adopted, were the difference in elevation between the considered point and the source of risk (*H*), and the distance from the nearest stream (*D)*. These features have been also applied in the present study case with a number of additional morphological indices. Results highlighted remarkable differences in the performances of indices and features applied in different contexts. The study allowed to better address the sensitivity of each index with the change of scale, spatial resolution, etc.

2 STUDY AREA

The Bradano River is one of the major rivers of the Basilicata Region (southern Italy), with a drainage area of about 2,765km². The climate is characterized by a dry-sub humid regime with scarce rains and zero base flow during the summer period (see Fiorentino et al., 2007). More than the 77% of the total surface is covered by agricultural areas, and only the 23% by woodlands and semi-natural areas (this information is provided by the CORINE-Land Cover map of the European Environmental Agency). The upper basin is characterized by a marked topography; by contrast, the terminal portion of the basin, close to the outlet, is extremely flat.

This river basin is one of the most critical in terms of flooding for both the Basilicata and the contiguous Puglia Region. It produced several floods, causing significant damages especially in the portion of the basin close to the river outlet to the Ionian Sea. The first documented flood of the Bradano River refers to the 1827, when two bridges were destroyed interrupting the connection from the South to the City of Matera (this historical event is documented in the archives of the Kingdom of the Two Sicilies under Ferdinando II). Later on, a dramatic event occurred in 1959 when the cities near the coast were significantly damaged and several buildings were destroyed. More recently, flooding also occurred in 1972, 2004 and 2011 (see Figure 1), producing inundations in the outlet portion of the river basin, which is characterised by gentle slopes and flat surfaces. Some additional information on the damages produced by most of these events can be found on http://www.evalmet.it/.

3 METHODS AND DATASETS

3.1 Flood Maps

The extent of the inundated areas was studied by the River Basin Authority of Basilicata (RBAB), that mapped all the rivers of this region. The complex morphological characteristics of the basin forced the RBAB to use both one-dimensional (1D) and two-dimensional (2D) hydraulic models for flood mapping. The first was used for flood propagation along the main river, while the 2D model application was limited to a smaller portion of the river basin nearby the outlet (about 80km^2) characterised by extremely flat surfaces, in order to reduce the computational efforts.

Two-dimensional models allow studying flood propagation in the areas where it is not possible to recognize a prevailing direction of the water flow. Nevertheless, these models are computationally intensive and for this reason their application is generally limited to a portion of a river basin, while 1D models allow providing a more extensive description of the flood extent at the basin scale. In fact, in the present case the evaluation of the flood-prone areas for a given return period for the main river was carried out by the use of the HEC-RAS model (HEC-RAS, 2010), which is less reliable when dealing with the flat portion of the river basin. Therefore, the basin outlet was investigated by using a 2D approach. Both maps were obtained using a synthetic hydrograph derived from regional analyses assuming a return period of 30 years. The flood peak was calculated using the VAPI methodology (Claps et al., 1999), while the synthetic hydrograph was obtained exploiting the synthetic flow hydrograph proposed by NERC (1975) and modified by Fiorentino & Margiotta (1999).

It is necessary to remark that the RBAB’s studies are limited to a portion of the basin that includes the main River, but several tributaries are not analyzed. Therefore, it is highly desirable to have a tool able to provide an extensive characterization of the flood hazard over the entire river network. With this aim, we explored the use of binary classifiers exploiting the two flood maps that refer to the same basin, but differ for reference scale, DEM resolution and methodology adopted for flood mapping.

In order to clarify the procedure used by the RBAB to delineate flood maps, it is useful to provide some additional information about the models adopted. One model is HEC-RAS that probably does not require further descriptions, being a widely used software well documented on the web page of US army Corps of Engineers (http://www.hec.usace.army.mil). On the contrary, it seems appropriate to provide additional information about the 2D hydraulic model named FLORA-2D (FLOod and Roughness Analysis) recently introduced by Cantisani et al. (2012, 2014).

3.2 FLORA-2D

FLORA-2D was developed recently within a collaboration between the University of Basilicata and the company “Research on Energy System” (RSE spa). It has been developed with the aim to simulate flood propagation in flat areas taking into consideration the dynamic effect of vegetation. In fact, flow resistance due to vegetation can be a dominant factor in the inundation process for relatively shallow inundation (<1 m).

FLORA-2D has the capability to simulate the inundations considering the spatial and temporal variation of the resistance due to vegetation. Each node of the computational matrix has a roughness coefficient depending on the type of vegetation, flow depth and velocity. In particular, the Manning coefficient n is calculated according to Petryk and Bosmajian (1975) when the vegetation is rigid, and Freeman et al. (2000) in the case of flexible vegetation. The general algorithm governing the flood propagation is based on the “shallow water equations” simplified by neglecting the convective terms.

The model has been validated over the Bradano river using flood maps obtained from satellite data. This kind of procedure is becoming more common with the increased potentials of remote sensing products (see e.g., Frappartet al., 2005; Iacobellis et al., 2013, Domeneghetti et al., 2014). An example of a remote sensed image for the flood event of March 2011 is given in Figure 1.A, which has been used by Cantisani et al. (2014). Model reliability has been further investigated using for comparison the model Mike21 HD by the Danish Hydraulic Institute, FLO-2D by O'Brien (2007), FLATModel by Medina et al. (2007). In all cases, the results were comparable in terms of flood extent, but with the great advantage of a significant reduction of the computational costs.

In the present application, the computational domain was defined by a square grid with resolution of 10m, while the time step was set to 2sec. This resolution provides a good compromise between simulation time and data accuracy for a correct representation of the process (Sole et al., 2011). It was also observed that the time step of 2s ensures the model stability.

The above-mentioned hydrograph was assigned as upstream boundary condition, while a constant water level equal to 0.5 m a.s.l. was considered as downstream boundary condition (the sea level is assumed slightly above the ordinary conditions). Finally, the spatial distribution of the flow resistance was derived from LiDAR data, used to generate maps of vegetation height (Cobby et al., 2001).

3.3 Digital Elevation Models

Digital Elevation Models (DEMs) contain a significant amount of information that may be helpful for the delineation of flood-prone areas (see e.g., Manfreda et al., 2014).

In the present case, we used, for the entire river basin, the USGS HydroSHEDS (Hydrological data and maps based on SHuttle Elevation Derivatives at multiple Scales-hydrosheds.cr.usgs.gov/index.php) elevation data, available for the entire globe at a fairly good resolution; instead for the portion of the basin outlet we adopted a high resolution LIDAR-derived DEM.

Figure 2 provides a graphical description of the investigated area; in particular, Figure 2.A describes the digital elevation model of the Bradano river basin (called SRTM DEM), extracted from HydroSHEDS (hydrosheds.cr.usgs.gov/index.php) and Figure 2B shows the digital elevation model at the outlet (called LiDAR DEM) of the same basin, extracted from a LiDAR high-resolution DEM and resampled to a 10m x 10m grid.

HydroSHEDS DEMs are derived from remote sensed elevation data of the NASA Shuttle Radar Topography Mission (SRTM). The original SRTM data have been conditioned using a sequence of automated procedures: a DEM–VOID has been released, where the no-data voids have been filled and the main elevation inconsistencies removed. Furthermore, a DEM–CON is also available for hydrological applications; it has been further conditioned in order to accurately reproduce the actual river network. The conditioning process alters the original elevation data and this limits the use of the DEM–CON to drainage network identification procedures. Both the mentioned DEMs have been used for the Bradano River, with a resolution of 3 arc-second that corresponds, for the current study area, to a square grid size of about 90m.

The LiDAR high-resolution DEM, instead, was obtained combining airborne LiDAR survey and field measurements that were carried out specifically for the RBAB, paying particular attention to position and elevation of levees. The laser scanning survey was carried out with a density of point equal to 0.7 points/m^2.

Figure 3 provides a representation of the standard flood maps used as reference for the application of the linear binary classification. In particular, Figure 3.A shows a flood map derived using a one-dimensional approach over the entire Bradano River, instead Figure 3.B provides a representation of the flooded areas identified by the application of the FLORA-2D model at the outlet of the Bradano basin.

3.4 LINEAR BINARY CLASSIFIERS AND ROC ANALYSIS

Techniques of pattern classification are used to compare DEM-derived quantitative morphologic features and existing flood hazard maps. The linear binary classifiers represent a useful tool for the scope, allowing a quantitative comparison between two binary maps (see Degiorgis et al., 2012). In particular, the flooded areas are easily converted into a binary map assigning a code 1 for flooded areas and a code 0 for marginal hazard areas. The marginal hazard areas are introduced in order to identify the portion of the river basin where a clear distinction between flooded and non-flooded areas is possible. The comparison with morphological features is possible imposing a threshold value to distinguish between the two possible values of the map. In this scheme, the threshold value becomes a parameter that may be changed in order to optimize the performance of each feature.

Binary classifiers need to be trained. For this reason, areas predicted as flooded by the use of hydraulic models (one-dimensional over the entire Bradano basin and two-dimensional at the outlet) are used to calibrate the optimal threshold that allows to distinguish flood-prone areas for each selected feature.

Single and composite morphologic features are scaled in normalized features lying between -1 and 1. Different normalized thresholds are applied to each normalized features obtaining a binary map of 0 and 1. Comparing this map with the flood map obtained by the hydraulic model, there are four possible conditions in each point of the map: if the threshold detects a flooded area when this condition is present, the point is counted as a true positive; otherwise, if it classifies a point as non-flooded (negative), it is counted as a false negative. If the site is defined non-flooded by the inundation map and it is classified as negative, it is counted as a true negative; otherwise, if it is classified as positive, it is counted as a false positive.

The quality of each binary classifier is evaluated using the Receiver Operating Characteristic (ROC) curves that represent a good measure of performance. The ROC graphs are obtained by varying the threshold of the classifier and are defined as the set of pairs of true positive rate (plotted on the Y axis) and false positive rate (plotted on the X axis). ROC curves are also used to select a suitable threshold value (see Fawcett, 2006).

We recall that the true positive rate (also called hit rate) is estimated as:

$$r_{tp} \approx \frac{Positives\ correctly\ classified}{Total\ positives} \qquad [1]$$

The false positive rate (also called false alarm rate) of the classifier is:

$$r_{fp} \approx \frac{Negatives\ incorrectly\ classified}{Total\ negatives} \qquad [2]$$

The diagonal line y = x represents the strategy of randomly guessing a class. Any classifier that appears in the higher left triangle performs better than random selection. The best value of the normalized threshold is obtained by minimizing the sum of the false positive rate and the false negative rate $r_{fp} + (1 - r_{tp})$ assigning equal weights to the two rates.

In order to compare different kinds of binary classifiers, a common method to reduce ROC performance to a single scalar value is to calculate the Area Under the ROC Curve, abbreviated AUC. The value of the AUC ranges from 0.5 (completely random classifier) to 1.0 (perfectly discriminating classifier).

3.4.1 SINGLE FEATURES

In the present section, we provide a synthetic description of the DEM-derived morphologic features adopted in the present study. Among all possible features, we considered the same list adopted by Degiorgis et al. (2012):

1. the upslope contributing area, A_s [m^2];

2. the surface curvature, $\nabla^2 H$ [-], defined as the Laplacian of the elevation;

3. the local slope, S [-], estimated as the maximum slope among the eight possible flow directions that connect the cell under exam to the adjacent cells;

4. the distance from the nearest stream, D [m], defined as the length of the path that hydrologically connects the location under exam to the nearest element of the reference drainage network;

5. the elevation to the nearest stream, H [m], computed as the difference between the elevation of the cell under exam and the elevation of the final point of the above-identified path.

A description of these features computed for the Bradano River Basin is given in Figure 4, where one can observe the plots obtained using the DEM at 90m of resolution in Figure 4.A (for the entire basin), while the features obtained for the basin outlet with a DEM at 10m of resolution are given in Figure 4.B. It is necessary to specify that in this last case features like the contributing area have been corrected in order to avoid border effects assigning to the channel cells on the border values derived from the larger DEM.

3.4.2 COMPOSITE INDICES

In addition to the mentioned features, a number of composite indices have been also used. Some of these indices are taken from the literature and others have been defined with the aim to describe the relative distance between the water surface during a flood and the local elevation (see Manfreda et al., 2014b). In particular, we adopted the following indices:

- The modified topographic index, TI_m, first introduced by Kirkby (1975), has proven to be a good indicator for the delineation of areas exposed to flood inundation (Manfreda et al., 2011). This index takes the form:

$$TI_m = \ln\left(\frac{A_d^n}{\tan(\beta)}\right), \qquad [3]$$

where A_d [m]is the drained area per unit contour length, tan(β) is the local gradient, n is an exponent <1.

- The downslope index, DW_i, proposed by Hjerdt et al. (2004) represents a new way of estimating the hydraulic gradient. The method does not use the exit point at the stream as reference; instead, it calculates how far (L_d [m]) a parcel of water has to travel along its flow path to lose a certain amount of potential energy (d [m]). This index is defined as:

$$\tan(\alpha_d) = \frac{d}{L_d}, \qquad [4]$$

where d was set equal 5m in the present case.

- H/D: it is obtained by calculating the ratio between the flow distance D and elevation difference H.

- ln[$h(A_s)/H$]: this index aims to compare in each point a variable water depth h with the elevation difference H, where h is calculated for each basin cell assuming a scaling relationship with the contributing area (A_s) by using an hydraulic scaling relation:

$$h(A_s) \approx A_s^n, \qquad [5]$$

where h is the water depth [m], $A_s$is the upslope contributing area at the point of interest [m^2], n is the exponent (dimensionless) set equal to 0.3 (see e.g. Nardi et al., 2006).

- ln[$h(A_r)/H$]: this index is similar to the previous one, but in this case h is computed as a function of the contributing area A_r in the section of the drainage network hydrologically connected to the point under exam (see figure 4).

- $[h(A_r) - H]/\ tan(\alpha_d)$: this index aims to describe, in each point of the investigated basin, the change between water depth $h(A_r)$ and the elevation difference H divided by a surrogate of the hydraulic gradient represented by the downslope index.

- $[h(A_r) - H]/D$: this index aims to describe, in each point of the investigated basin, the change between water depth $h(A_r)$ and the elevation difference H divided by the distance D.

All the indices and features are standardized in order to assume a value included in the range -1 and 1.

Figure 6 provides a visual description of the introduced indices computed for the entire Bradano River basin (A) and the Bradano outlet (B). It is necessary to state that the present list of indices was developed by the authors with the specific aim of identifying an hydraulic metric able to account for the main features affecting flood diffusion on the landscape. These indices have been tested also on the Tiber River in Manfreda et al. (2014b).

4 RESULTS AND DISCUSSION

All suggested features and composite indices have been used to explore their individual ability to describe flood hazard in the Bradano River basin. Given the strong morphological differences existing between the main river and its terminal part, it is extremely interesting to compare the performances of indices applied over the two areas.

Figures 7 and 8 show respectively the ROC curves obtained by separately thresholding each feature on the proposed study area for the two datasets previously introduced. In Figures 7, ROC curves are obtained by comparing the proposed features with the flood map of the Bradano basin obtained by using a 1-D hydraulic model, while in Figure 8 by comparing the proposed features with the flood map of the outlet of Bradano basin evaluated using a 2-D hydraulic model. Generally, the best performing parameters are those that minimize the area above the curve or maximize the area under the curve.

The visual comparison of all ROCs highlights the potential of each feature or index in delineating the flood-prone areas in different contexts. The inter-comparison of the four panels presented in Figure 7 and 8 allow stating that:

i. Among all single features considered the difference in elevation between the considered point and the source of risk (H), and the distance from the nearest stream (D) generally perform better. In fact, the ROC curve of such features has a very large AUC in the first area (Figure 7A).

ii. The behaviour of single features is different in the two considered study cases. In particular, they lower significantly their performances when applied to the flat area of the basin outlet (see Figure 8A).

iii. Among the composite indices, the best performing ones are the $\ln(h(A_s)/H)$ and the $\ln[h(A_r)/H]$ indices for the main river (application of 1-D hydraulic model over the entire Bradano river) and $\ln[h(A_r)/H]$ and $[h(A_r) - H]/D$ indices for the basin outlet (see Figure 7B and 8B).

iv. The composite index, $\ln[h(A_r)/H]$, provides similar performances in the two study areas considered herein, and therefore seems the most promising metric among those considered since now.

It is interesting to underline that the single features become less sensitive when dealing with a flat landscape and even features like H and D, that generally are well suited for flood mapping in several context, here seem to fail. The reason is certainly due to the specific morphological complexity of the area that probably cannot be characterized by this simple metric. On the other hand, the composite index, $\ln[h(A_r)/H]$, is able to reproduce closely the flood map derived both in the flat area and also over the entire river basin.

In order to provide a quantitative description of the quality of each classifier, we summarize in Tables 1 and 2 the performance of each feature computed for an optimal threshold value, considering the basin scale and the local scale of application, respectively investigated through the one-dimensional and two-dimensional approach. The optimal threshold values were identified by minimizing the sum of the false positive rate and the false negative rate $r_{fp} + (1 - r_{tp})$. In particular, Tables (1 and 2) provide the following information: the relative values of the optimal normalized threshold τ, the false positive rate r_{fp}, the true positive rate r_{tp}, the sum $r_{fp} + (1\text{-}r_{tp})$ and the area under the curve AUC for each of the presented features for the Bradano River basin.

Results show that the index ln[$h(A_r)/H$] is consistently one of the best performing indices in both cases. Furthermore, it is really remarkable that the thresholds identified for this index are similar in the two cases considered herein, while other features or indices show a larger variability of the performances and of the threshold values calibrated in the two considered cases. This result is particularly significant considering the change of scale of the two DEMs and also the reference hydraulic models adopted. This result may be somehow due to the fact that this index try to resample a physical property of flooding that is independent from the scale and the morphological characteristics of the study area. All this should be explored in additional study cases, but it is extremely stimulating if confirmed, because it would demonstrate the great advantage of this methodology, that could allow to extend the flood mapping over large areas starting from the study of a small portion of the basin and using any kind of hydraulic model for the calibration of the method.

An example of application of the procedure over the Bradano River basin is given in Figure 9A and B, where we identified the portion of the basin that have a value of the ln[$h(A_r)/H$] index above the calibrated threshold. The maps obtained using the ln[$h(A_r)/H$] index provided good performance in both the analysed contexts. After the calibration of the optimal thresholds of this index, the flood hazard has been extended over all tributaries, obtaining a realistic description of the flood prone areas that may be extremely useful for the local River Basin Authority to extend their knowledge about flood hazard.

5 CONCLUSION

The present study investigates the role of different morphological descriptors in the identification of flood-prone areas over the Bradano River basin. In particular, the performances of the proposed features are evaluated using a linear binary classifier and ROC analysis at two different scales of application: at the entire basin scale, using for comparison a flood map derived by a one-dimensional simulation, and in a flat zone of the river basin, exploiting a flood map derived by a two-dimensional model (FLORA-2D). Among the local features, the best performing ones are the difference in elevation between the considered point and the source of risk (*H*), and the distance from the nearest stream, *D*; instead, among the composite indices the ones performing better are the $\ln[h(A_s)/H]$ and $\ln[h(A_r)/H]$. In particular, this last seems to be more consistent and less sensitive to the change of resolution in the adopted DEM, the reference hydraulic map used for calibration, and the different topography of the training area. It also provides a reliable representation of the flood-prone areas even in the case of flat areas, where other indices or features become less and less sensitive. The outcomes of the present study are particularly promising, especially considering the number of artificial modifications that characterize the Bradano River.

Acknowledgements: We would like to acknowledge the valuable contribution of the two anonymous reviewers. This research was carried out within the framework of activities of the CINID under the research agreement with the Civil Protection of the Basilicata Region.

REFERENCES

Bridgham SD, Cadillo-Quiroz H, Keller JK, & Zhuang Q (2013) Methane emissions from wetlands: Biogeochemical, microbial, and modeling perspectives from local to global scales. Global Change Biology, 19(5), 1325–1346.

Brivio PA, Colombo R, Maggi M & Tomasoni R (2002) Integration of remote sensing data and GIS for accurate mapping of flooded areas, International Journal of Remote Sensing, 23:3, 429-441, DOI: 10.1080/01431160010014729.

Cannon T (1994) Vulnerability analysis and the explanation of "natural" disasters, in A. Varley (ed.) Disasters, development and the environment, Chichester: John Wiley.

Cantisani A (2012). Monitoraggio e modellazione per la protezione dal rischio idraulico in aree pianeggianti mediante lo sviluppo e l'applicazione di modelli bidimensionali e l'utilizzo di strumenti GIS Open Source (Università della Basilicata).

Cantisani A, Giosa L, Mancusi L, Sole A, (2014) FLORA-2D: A New Model to Simulate the Inundation in Areas Covered by Flexible and Rigid Vegetation. *International Journal of Engineering and Innovative Technology*, vol. 3, Issue 8, p. 179-186, ISSN: 2277-3754.Ceola S, Laio F, Montanari A, (2014) Satellite nighttime lights reveal increasing human exposure to floods worldwide, Geophysical Research Letters, Volume 41, Issue 20, pages 7184–7190, 28 October 2014.

Claps P, Fiorentino M., Rapporto di sintesi sulla valutazione delle piene in Italia – Guida Operativa all'applicazione dei rapporti regionali sulla valutazione delle piene in Italia, 1999, Linea 1 Previsione e Prevenzione degli eventi idrologici estremi. CNR – GNDCI Roma.

Cobby DM, Mason DC, Davenport IJ, (2001) Image processing of air born scanning laser altimetry for improved river flood modelling, ISPRS Journal of Photogrammetry and Remote Sensing, 56(2): 121-138.

De Risi R., Jalayer F., De Paola F. and Giugni M. (2014) Probabilistic delineation of flood-prone areas based on a digital elevation model and the extent of historical flooding: the case of Ouagadougou. Boletín Geológico y Minero,125 (3): 329-340 ISSN: 0366-0176.

Degiorgis M, Gnecco G, Gorni S, Roth G, Sanguineti M, Taramasso AC (2012) Classifiers for the detection of flood-prone areas using remote sensed elevation data. *J. Hydrol*., 470-471, 302–315.

Domeneghetti A, Tarpanelli A, Brocca L, Barbetta S, Moramarco T, Castellarin A, Brath A (2014). The use of remote sensing-derived water surface data for hydraulic model calibration. Remote Sensing of Environment 149, (2014), 130–141.

Douglas I, Alam K, Maghenda M, Mcdonnell Y, Mclean L and Campbell J, (2008) Unjust waters: climate change, flooding and the urban poor in Africa, Environment and Urbanization 20: 187, DOI: 10.1177/0956247808089156.

Fawcett T (2006) An introduction to ROC analysis. *Pattern Recognit. Lett*. 27, 861–874.

Fiorentino M, Manfreda S, Iacobellis V (2007) Peak Runoff Contributing Area as Hydrological Signature of the Probability Distribution of Floods. *Adv. Water Resour*., 30(10), 2123-2134.

Fiorentino M, Margiotta MR (1999) La valutazione dei volumi di piena ed il calcolo semplificato dell’effetto di laminazione di grandi invasi, Atti del 19° corso di aggiornamento su "Tecniche per la difesa dall'inquinamento, G. Frega (a cura di), Editoriale Bios, Cosenza, 203-222.

Fluet-Chouinard E, Lehner B, Rebelo L-M, Papa F, and Hamilton SK, (2014) Development of a global inundation map at high spatial resolution from topographic downscaling of coarse-scale remote sensing data, Remote Sensing of Environment, http://dx.doi.org/10.1016/j.rse.2014.10.015

Frappart F, Seyler F, Martinez J-M, León J G, Cazenave A, (2005) Floodplain water storage in the Negro River basin estimated from microwave remote sensing of inundation area and water levels, Remote Sensing of Environment, 99(4), 387--399 http://dx.doi.org/10.1016/j.rse.2005.08.016.

Freeman GE, Rahmeyer W, Copeland R R (2000) Determination of Resistance Due to Shrubs and Woody Vegetation, Coastal and Hydraulics Laboratory, ERDC/CHL TR-00-25, U.S. Army Engineer.

HEC-RAS 4.1: online available at: http://www.hec.usace.army.mil/software/hec-ras/documentation/HEC-RAS_4.1_Reference_Manual.pdf.

Hjerdt KN, McDonnell JJ, Seibert J, Rodhe A (2004). A new topographic index to quantify downslope controls on local drainage. Water Resour. Res., 40, W05602.

Iacobellis V, Gioia A, Milella P, Satalino G, Balenzano A and Mattia F (2013) Inter-comparison of hydrological model simulations with time series of SAR-derived soil moisture maps. European Journal of Remote Sensing- 46: 739-757; doi: 10.5721/EuJRS20134644.

Jalayer F, De Risi R, De Paola F, et al. (2014) Probabilistic GIS-based method for delineation of urban flooding risk hotspots, *Natural Hazards*, ISSN: 0921030X, DOI: 10.1007/s11069-014-1119-2.

Kirkby MJ (1975) *Hydrograph modelling strategies*, Progress Phys. Hum. Geogr., 69–90.

Manfreda S, Di Leo M, Sole A (2011) Detection of Flood Prone Areas using Digital Elevation Models. *J. Hydrol. Eng*., 16(10), 781-790.

Manfreda S, Nardi F, Samela C, Grimaldi S, Taramasso AC, Roth G and Sole A, (2014a) Investigation on the Use of Geomorphic Approaches for the Delineation of Flood Prone Areas, *J. Hydrol*., 517, 863-876.

Manfreda S, Samela C, Sole A, and Fiorentino M (2014b) Flood-Prone Areas Assessment Using Linear Binary Classifiers based on Morphological Indices. Vulnerability, Uncertainty, and Risk: pp. 2002-2011. doi: 10.1061/9780784413609.201.

Medina V, Hurlimannn M, Bateman A, Application of FLATModel, a 2D finite volume code, to debris flows in the northeastern part of Iberian Peninsula, Landslides, Springer Verlag Editor, 2007.

Milly PCD, Wetherald RT, Dunne KA, Delworth TL (2002) Increasing risk of great floods in a changing climate. Nature, 415, 514-517.

Nardi F, Vivoni ER, Grimaldi S (2006) Investigating a floodplain scaling relation using a hydrogeomorphic delineation method. Water Resour. Res., 42, W09409.

Nel JL, Roux DJ, Abell R, Ashton PJ, Cowling RM, Higgins JV, Thieme M, Viers JH (2009) Progress and challenges in freshwater conservation planning. Aquatic Conservation: Marine and Fresh water Ecosystems, 19(4), 474–485.

O'Brien J, FLO-2D User Manual. Version2007.06.

Papaioannou G, Vasiliades L, Loukas A (2014) Multi-Criteria Analysis Framework for Potential Flood Prone Areas Mapping, J Water Resources Management, Springer Netherlands, http://dx.doi.org/10.1007/s11269-014-0817-6.

Petryk S, Bosmajian G B (1975) Analysis of flow through vegetation, Journal of the Hydraulics Division, ASCE, 101(7): 871-884.

Prudhomme C, Reynard N and Crooks S (2002) Downscaling of global climate models for flood frequency analysis: where are we now?, Hydrol. Process. 16, 1137–1150.

Sharitz RR, Mitsch WJ (1993) Southern hardwood forests. In: Martin, W.H., Boyce, S.G., Echtemacht, A.C. (Eds.), Biodiversity of the Southeastern United States: Lowland Terrestrial Communities. Wiley, New York, pp. 311-372.

Sole A, Giosa L, Cantisani A, Statuto D, Nolè L (2011) Analisi di sensibilità nella modellazione delle inondazioni di aree pianeggianti - Sensitivity analysis in flood modeling of flat areas, Italian Journal of Engeneering Geology and Environment, Special Issue, pp. 157-167, DOI: 10.4408/IERGE. 2011-01.S-12.

Townsend PA, Walsh SJ, (1998) Modeling floodplain inundation using an integrated GIS with radar and optical remote sensing, *Geomorphology*, Volume 21, Issues 3–4, January 1998, Pages 295-312, ISSN 0169-555X, http://dx.doi.org/10.1016/S0169-555X(97)00069-X.

EntireBradanoBasin - 1D Hydraulic Model					
Single features	**τ**	**r_{fp}**	**r_{tp}**	**r_{fp}+(1-r_{tp})**	**AUC**
A_s	-0.999	0.021	0.186	0.834	0.584
D	**-0.928**	**0.178**	**0.784**	**0.395**	**0.882**
ΔH	0.051	0.627	0.897	0.730	0.578
H	**-0.960**	**0.113**	**0.963**	**0.150**	**0.964**
S	-0.956	0.286	0.898	0.388	0.870

Indices	**τ**	**r_{fp}**	**r_{tp}**	**r_{fp}+(1-r_{tp})**	**AUC**
Tim	-0.235	0.286	0.899	0.387	0.869
DW_i	-0.980	0.142	0.883	0.259	0.919
H/D	-0.974	0.272	0.812	0.460	0.841
ln[h(A_r)/H]	**-0.422**	**0.143**	**0.939**	**0.204**	**0.950**
ln[h(A_s)/H]	**-0.612**	**0.134**	**0.953**	**0.182**	**0.953**
[h(A_r)-H]/DW_i	-0.991	0.790	0.992	0.799	0.654
[h(A_r)-H]/D	0.818	0.133	0.874	0.259	0.933

Table 1. Results of the linear binary classifiers for the Bradano River basin: the optimal normalized threshold, τ, the false positive rate, r_{fp}, the true positive rate, r_{tp}, the sum $r_{fp} + (1 - r_{tp})$, and the area under the curve (AUC) for each descriptor. The best performing features are highlighted using bold characters.

Bradano Outlet - 2D Hydraulic Model					
Single features	**τ**	**r_{fp}**	**r_{tp}**	**r_{fp}+(1-r_{tp})**	**AUC**
As	-0.991	0.000	0.015	0.985	0.507
D	**-0.842**	**0.247**	**0.458**	**0.789**	**0.625**
ΔH	0.330	0.421	0.458	0.963	0.527
H	**-0.574**	**0.768**	**0.990**	**0.778**	**0.609**
S	-0.986	0.644	0.719	0.926	0.548

Indices	**τ**	**r_{fp}**	**r_{tp}**	**r_{fp}+(1-r_{tp})**	**AUC**
TIm	-0.139	0.453	0.531	0.922	0.555
DW_i	0.000	0.142	0.441	0.701	0.609
H/D	-0.755	0.911	0.992	0.919	0.505
ln[h(A_r)/H]	**-0.423**	**0.267**	**0.811**	**0.456**	**0.791**
ln[h(A_s)/H]	-0.809	0.759	0.956	0.803	0.623
[h(A_r)-H]/DW_i	-0.068	0.558	0.886	0.672	0.659
[h(A_r)-H]/D	**0.471**	**0.221**	**0.734**	**0.487**	**0.798**

Table 2. Results of the linear binary classifier for the outlet of Bradano River basin: the optimal normalized threshold value τ, the false positive rate r_{fp}, the true positive rate r_{tp}, the sum of r_{fp}+(1-r_{tp}) and the area under the curve (AUC) for each descriptor. The best performing features are highlighted using bold characters.

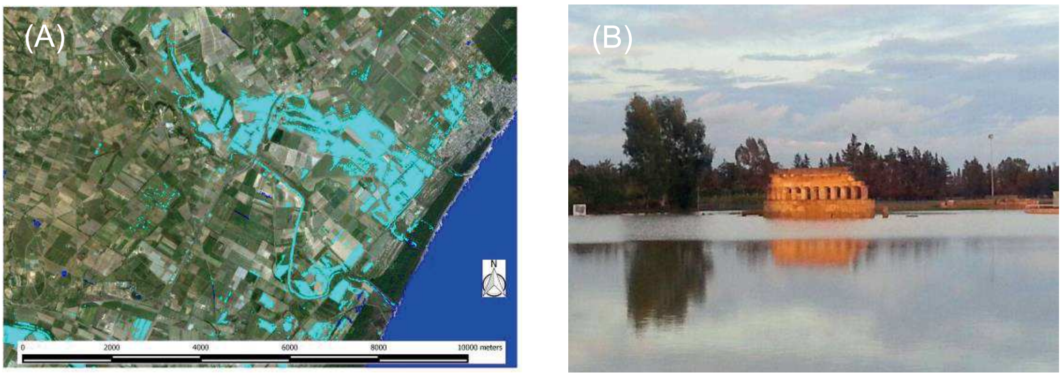

Figure 10. A) Inundated areas during the flood event of March 2011 obtained by processing remote sensed images. B) The Ancient Temple of “Tavole Palatine” flooded by the event of March 2011.

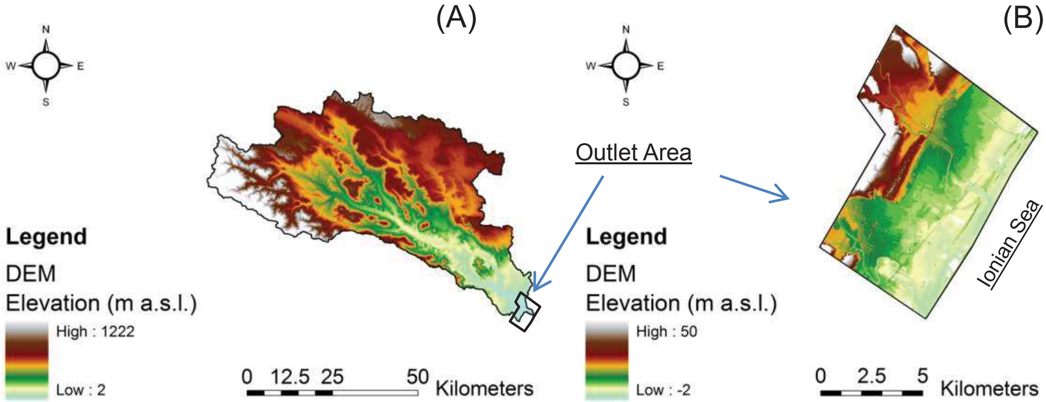

Figure 1. SRTM DEM of the entire Bradano River basin (A). LiDAR DEM of the basin outlet of Bradano River (B).

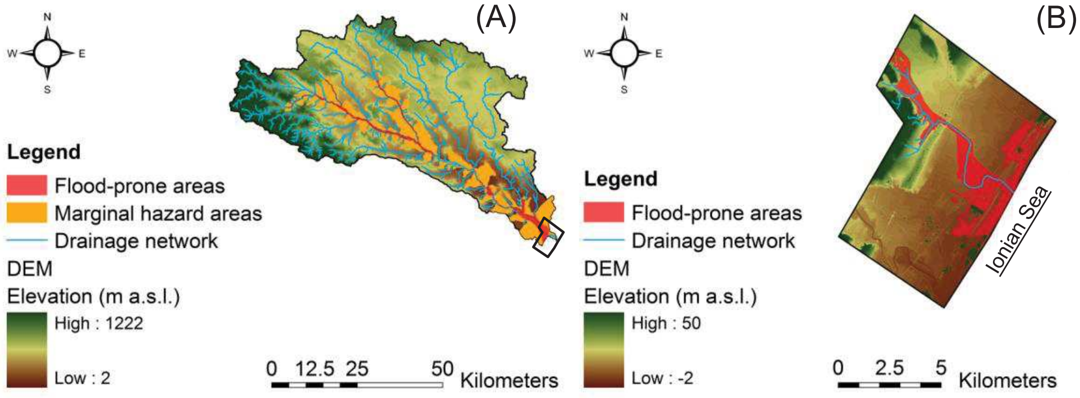

Figure 2. Flood map derived by using a one-dimensional approach over the entire basin of Bradano (A). Flood map derived by using a two-dimensional approach at the outlet of Bradano River basin (B).

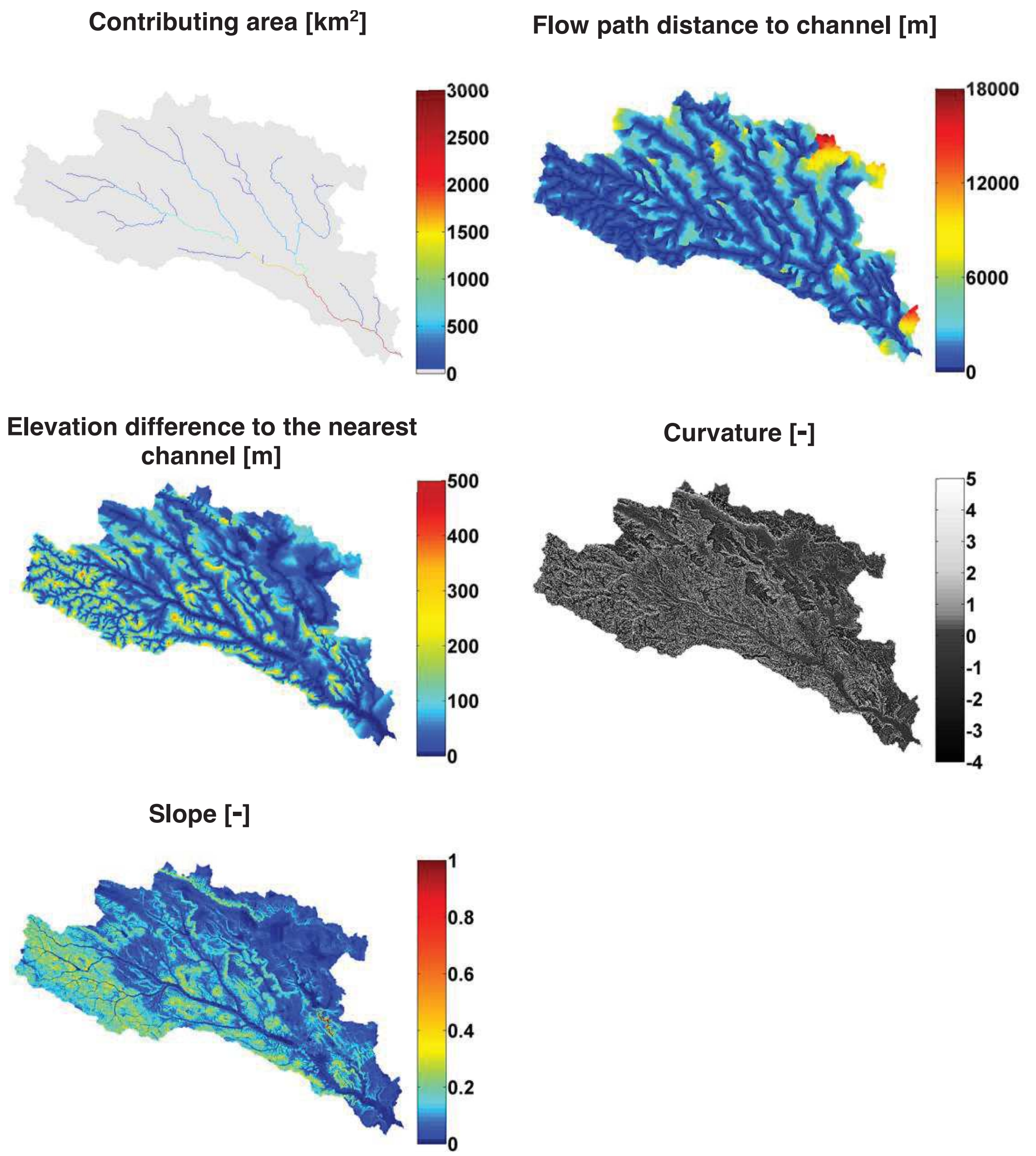

Figure 3A. Local morphological features estimated for the entire Bradano river basin using the SRTM DEM with 90 m of resolution.

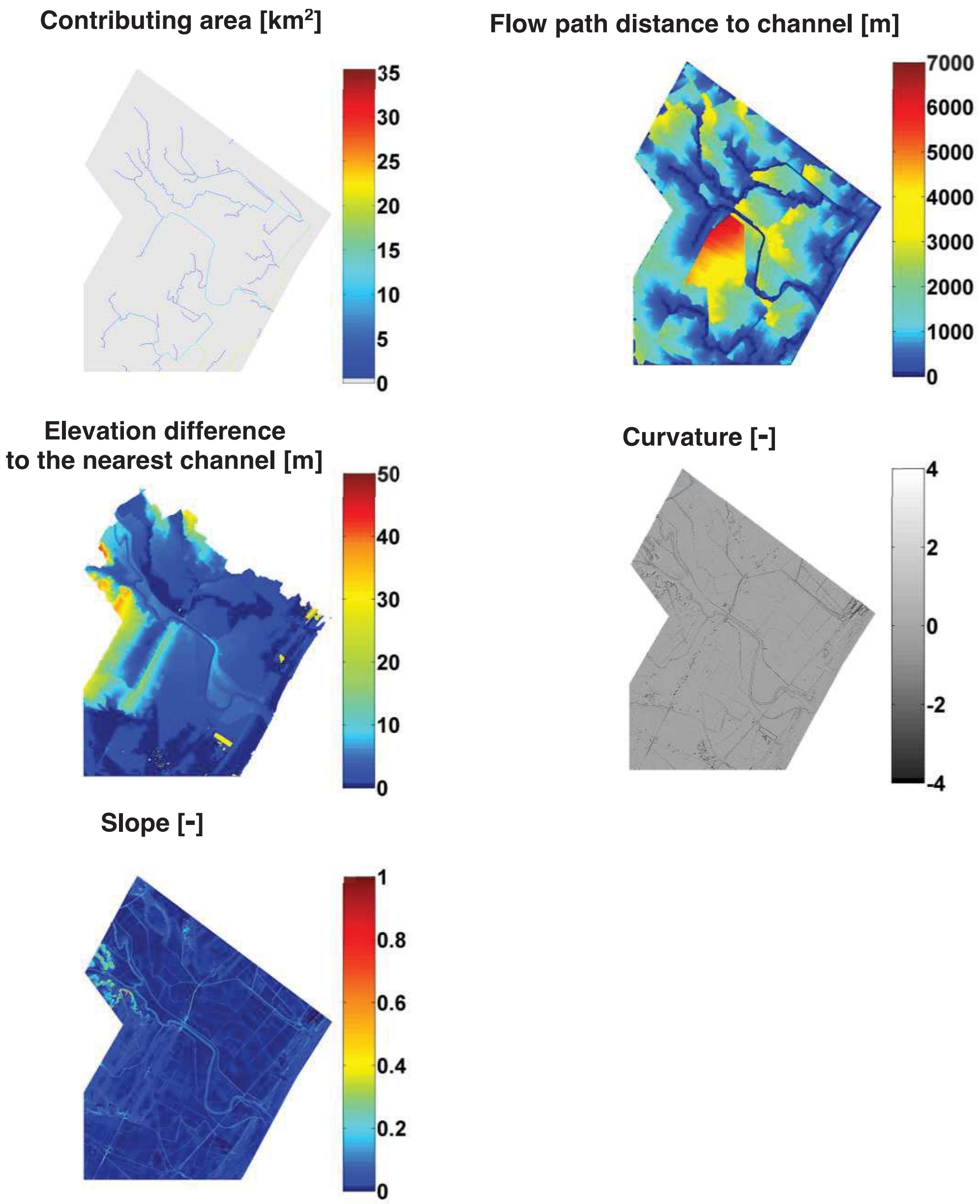

Figure 3B. Local morphological features calculated at the outlet of the Bradano basin estimated using the LiDAR DEM with 10 m of resolution.

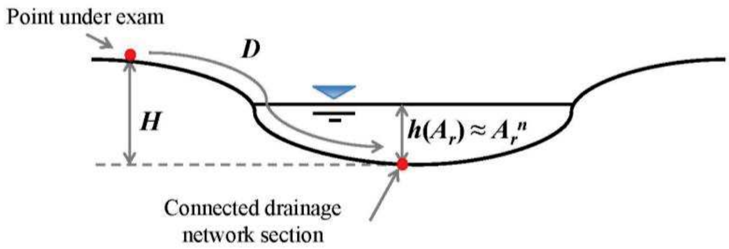

Figure 4. Example of a hydraulic cross-section with the description of the parameters *H* and *h*.

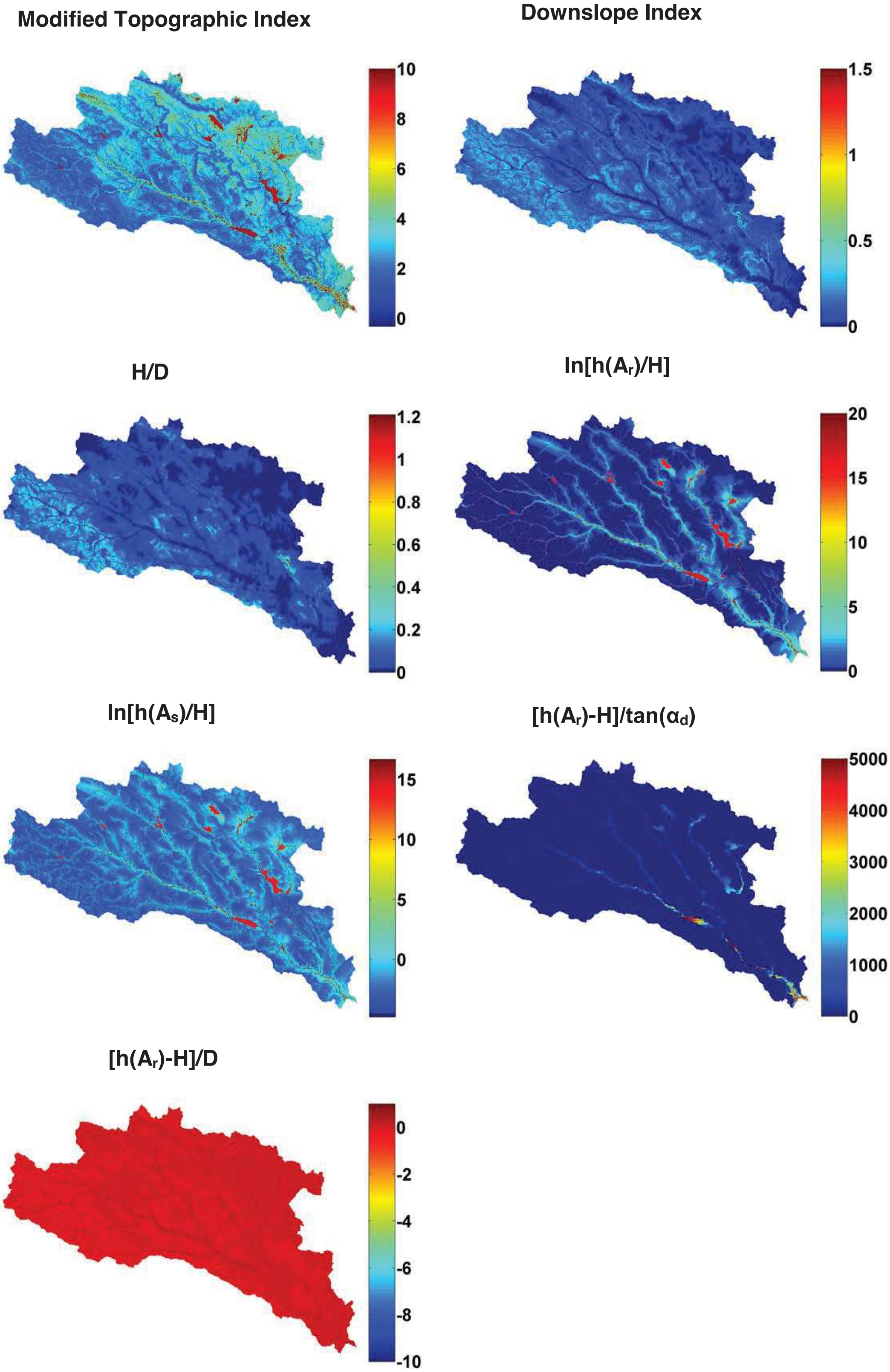

Figure 5A. Composite morphological indices estimated for the entire Bradano river basin using the SRTM DEM with 90 m of resolution.

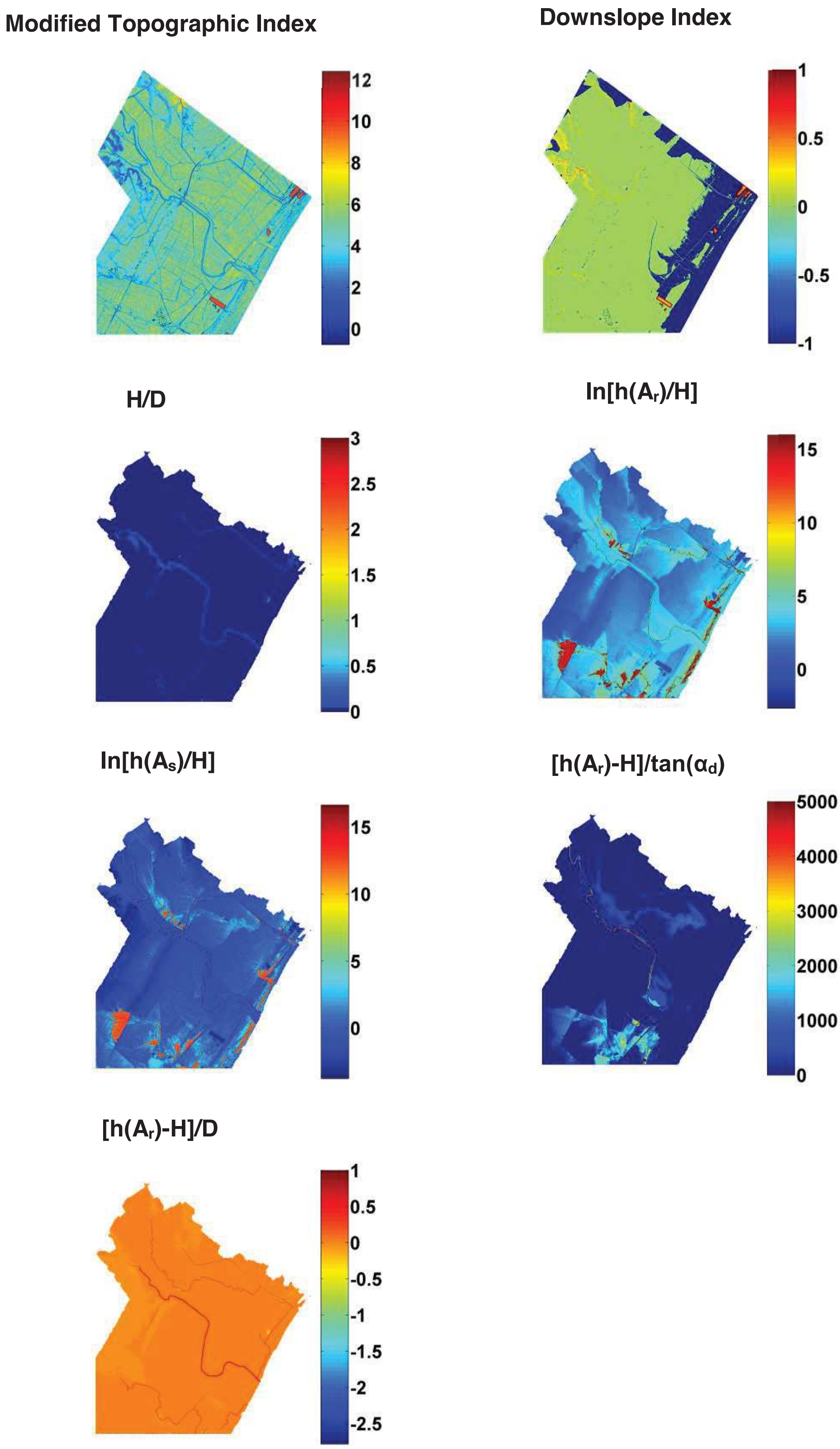

Figure 5B. Composite morphological indices computed at the outlet of the Bradano river basin estimated using the LIDAR DEM with 10 m of resolution.

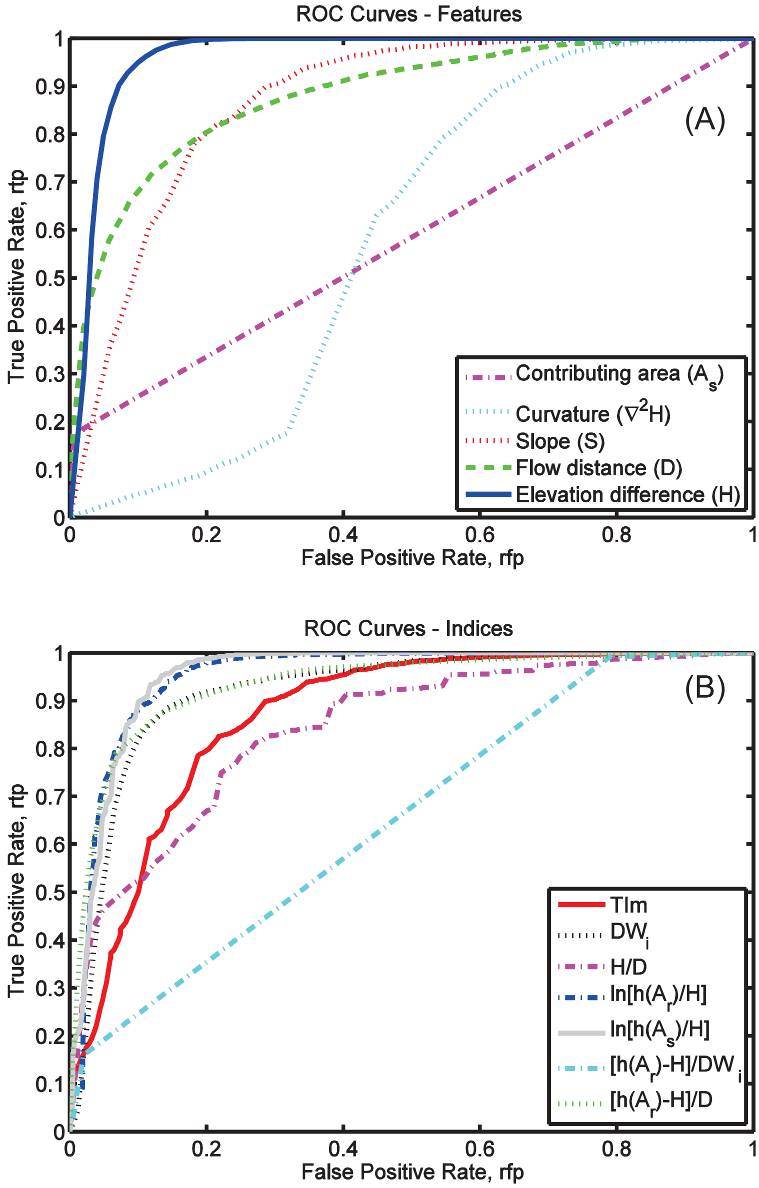

Figure 6. ROC curves obtained for local features (A) and composite indices (B) obtained by comparing the proposed features with the flood map of the Bradano basin obtained using the 1-D hydraulic model.

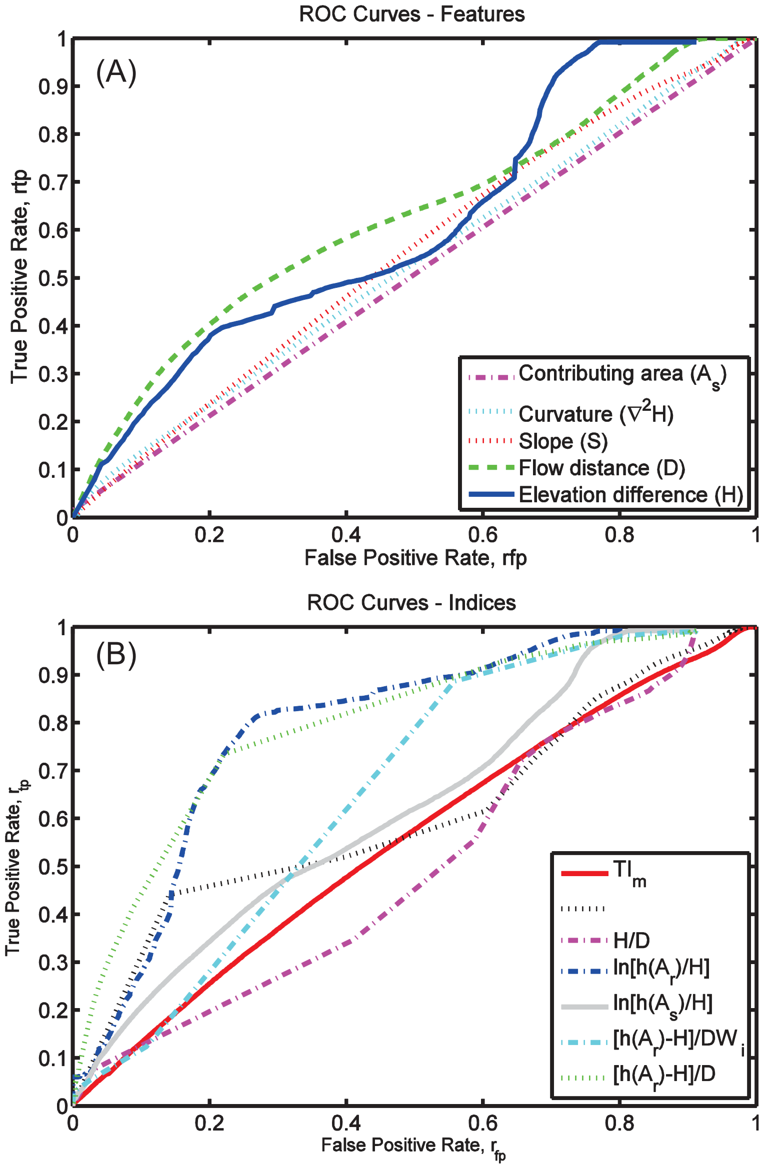

Figure 7. ROC curves obtained for local features (A) and composite indices (B) obtained by comparing the proposed features with the flood map of the outlet of Bradano basin evaluated using the 2-D hydraulic model.

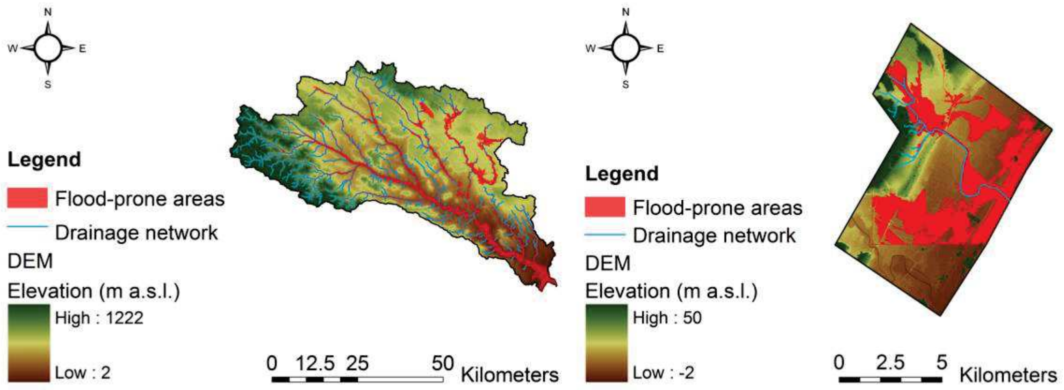

Figure 8. Flood maps of the Bradano River basin obtained using the linear binary classifier based on the index *$ln(h(A_t)/H)$* applied on the entire basin (A) and the basin outlet (B).

Additional Material for Editor and Reviewers

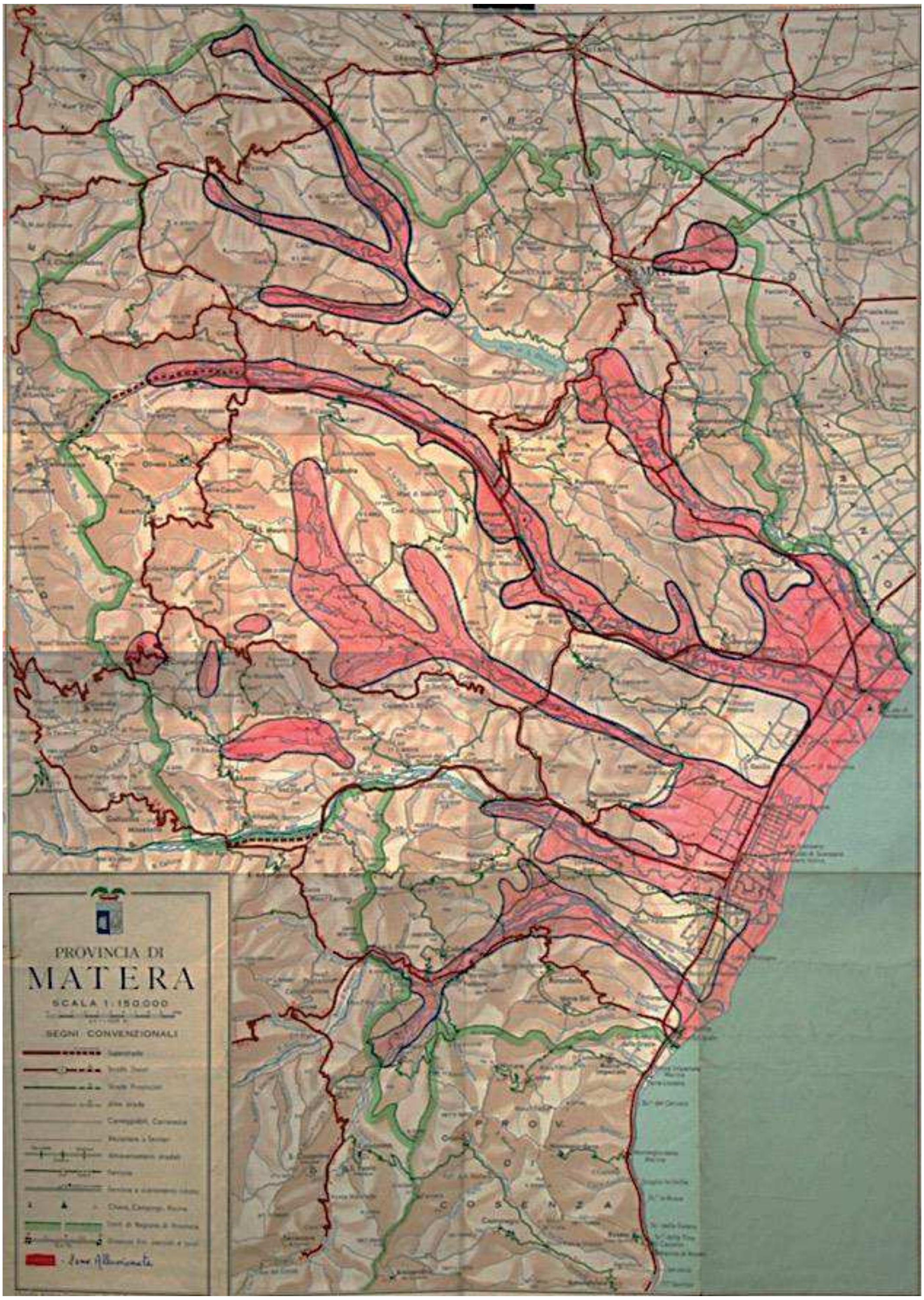

Figure 9. Inundated areas during the flood event of January 1972 edited by the Province of Matera.